Journal of Alloys and Compounds 960 (2023) 170695

Contents lists available at ScienceDirect

Journal of Alloys and Compounds

journal homepage: www.elsevier.com/locate/jalcom

Sustainable inorganic pigments with high near-infra-red reflectance based on Fe^{3+} doped $YAlO_3$ for high temperature applications

Silvia Blasco-Zarzoso, Héctor Beltrán-Mir *, Eloísa Cordoncillo *

Departamento de Química Inorgánica y Orgánica, Universitat Jaume I, Av. Sos Baynat s/n, 12071 Castellón de la Plana, Spain

ARTICLE INFO

Article history:
Received 27 March 2023
Received in revised form 17 May 2023
Accepted 21 May 2023
Available online 23 May 2023

Keywords:
Pigment
Near-infra-red reflectance
Coatings
Colour
Perovskite

ABSTRACT

Non-toxic inorganic pigments based on the Fe(III)-doped $YAlO_3$ with high near-infra-red (NIR) reflectance were synthesized by a modified Pechini method at 1200 °C. A complete solid solution in the $YAl_{1-x}Fe_xO_3$ system ($0 \leq x \leq 1$) was prepared, yielding a wide range of colourations from yellow to red, depending on the iron content.

Good pigment stability was achieved in a commercial high temperature glaze, used in the ceramic industry to colour glazes on tiles. The pieces coated with the pigmented glazes reached NIR solar reflectance values between 43% and 32%. The temperature protection studies carried out with the glazes pigmented with $YAl_{0.75}Fe_{0.25}O_3$ and $YFeO_3$ compositions, conclude that the pigmented samples reduce the temperature of a building by 5 °C and 4 °C, respectively, in comparison to the unpigmented glaze.

Thus, these pigments can be excellent candidates for used in high-temperature applications such as colouring ceramic high temperatures glazes, as well as cool pigments in walls or roofs of buildings.

1. Introduction

A significant amount of heat is absorbed through conduction in the surface of a material exposed to sunlight [1]. The solar spectrum can be divided into the ultraviolet (UV), visible (VIS) and near-infra-red (NIR) wavebands, these being about 5%, 43% and 52% of the total solar energy received by the earth, respectively [2]. Urban buildings consume large amounts of energy, especially by air conditioning which accounts for about 20% of global electricity consumption in buildings today. Furthermore, the demand for air conditioning is expected to increase in hotter regions, particularly in developing countries [3]. Saving in energy used for air-conditioning can be achieved by reducing the temperature of the building envelope, which in turn reduces the heat penetration into the building [4]. Therefore, to reduce energy used for air-conditioning, cooler roofs and walls can be used. Cooler roofs will reflect the sun's radiation, especially NIR radiation, and reduce the amount of energy absorbed by the building. Cool materials with high solar reflectance have been widely used as coatings on roofs and walls [5–7].

NIR-reflecting inorganic pigments have been incorporated in coatings applied to roofing products. Complex inorganic pigments with high NIR reflectance are based on mixed metal oxides like cobalt chromite green, cadmium stannate, strontium chromite yellow or chrome titanate yellow. All these pigments use toxic heavy metals [8]. Thus, research focuses on finding new non-toxic inorganic pigments with similar NIR reflectance for sustainable materials that reduce heat build-up while also enhancing their aesthetic appearance. It's important to consider both non-toxicity and colour characteristics to achieve an appealing appearance and high reflectance, particularly in the NIR region.

Most of the new inorganic pigments with high NIR reflectance found in the literature are based on rare earth and non-toxic transition metal oxides, therefore making them more environmentally friendly pigments [8]. It is important to highlight two non-toxic pigments currently used in the ceramic industry: Pr-zircon yellow [9,10] and Pr-cerianite reddish-brown [11,12]. These pigments will serve as a reference for comparison with the pigments prepared in this work. Among all these pigments, some of them used perovskites based on the $AFeO_3$ system, where A is a rare earth ion and iron is the non-toxic transition metal, but, in most of these studies, a single phase of perovskite is not achieved, which is an important aspect to consider when using the pigment for colouring different media, such as a ceramic glaze. However, it is important to point out that several commercial ceramic pigments, including those based on zircon or rutile, often exhibit residual phases to achieve a high pigmenting intensity [13]. Despite all of that, a comprehensive study of the

* Corresponding authors.
E-mail addresses: mir@uji.es (H. Beltrán-Mir), cordonci@uji.es (E. Cordoncillo).

https://doi.org/10.1016/j.jallcom.2023.170695

optical properties of the compounds has not been conducted in most of the work published to date.

The first work carried out in this field was mainly developed by Cunha in 2005 [14]. An orange compound ($LaFeO_3$) was synthesized using the Pechini method and calcination temperatures of 900ºC and 1100ºC, obtaining a single phase. Later, in 2008, pigments with the general formula $AFeO_3$ were obtained using lanthanides such as Gd, La, Yb, Tm and Lu, and prepared by the traditional ceramic method at temperatures of 900ºC and 1000ºC [15]. The authors of both papers indicated that the pigments darkened with increasing calcination temperature, possibly due to the partial reduction of Fe(III) to Fe(II), which affected the final colouration of the pigment. Later, Pieña et al. [16,17] used Mössbauer spectroscopy to verify that in the $AFeO_3$ compounds (*A*=Er, Sm, Nd, La and Ho) the oxidation state of iron did not vary, and the colouration of the pigments depended on the lanthanide used.

Over the years the research carried out to determine the chromatic coordinates of pigments also studied their reflectance, as for example in the $PrFeO_3$ perovskite synthesized by solid state reaction and calcined at a temperature of 1000ºC [18].

From then on, the study of the optical properties of pigments started to become more precise and in 2015, Liu et al. [19] reported yellow inorganic pigments based on the formula $LaFe_{1-x}Al_xO_3$ with high NIR reflectance at 700ºC. Replacing Fe^{3+} with Al^{3+} in this perovskite changed the colour from brown to yellow. The authors showed that the yellow pigments on galvanized sheets possessed an NIR solar reflectance of around 40%, and a temperature of around 5ºC could be controlled by using the yellow-coloured coatings in building roofing material. Yuan et al. [20], followed the same research method and synthesized reddish brown pigments with $Bi_{1-x}La_xFeO_3$ composition at 600ºC. The pigments yielded high reflectance in the NIR region. Recently, Li et al. [21] also reported the obtention of black and brown inorganic pigments with high NIR reflectance based on $YFeO_3$ perovskite at temperatures between 700ºC and 900ºC, in which the colour depended on the crystalline structure and the temperature. However, the temperature used in these studies, as well as in most of those indicated previously did not exceed of 1000ºC, and therefore, its viability for high-temperature applications such as the colouring of ceramic glazes for tiles has not been verified. It should be noted that despite the fact that in the work of reference 17 the pigments were prepared at temperatures reaching 1300 ºC, their viability in any application has not been studied.

Table 1 summarizes all the studies found in the literature using pigments with perovskite-type $AFeO_3$ structure calcined at different temperatures. As mentioned earlier, the low temperatures could be one of the reasons why the pigments have not been incorporated into ceramic glazes to date, as the pigment-frit mixture is fired at temperatures above 1000ºC.

From this point of view, it is worth mentioning the study carried out by Fortuño et al. [22], where the authors synthesized different perovskites with high near-infra-red (NIR) reflectance based on $AFeO_3$ (*A*=La, Pr, Nd, Sm, Gd, Tb, Y or Yb) at 1200ºC. All these pigments, which showed reddish hues, offered good colour stability after mixing them in powder form with siloxane transparent paint and two different glazes [22].

Table 1
Cited studies on pigments based on $AFeO_3$ stoichiometry.

Year	First author	*A* in $AFeO_3$	T (ºC)	Single phase	Ref.
2005	Cunha	La	900/1000	Yes	[14]
2008	Dohnalová	Gd/La/Yb/Tm/Lu	900/1000	No	[15]
2008	Pieña	La/Ho	1000	Yes	[16]
2010	Pieña	Er/Sm/Nd	1300	No	[17]
2015	Opuchovic	Ce/Pr/Nd/Tb	1000	No	[18]
2015	Liu	$LaFe_{1-x}Al_xO_3$	700	Yes	[19]
2018	Yuan	$Bi_{1-x}La_xFeO_3$	600	No	[20]
2021	Li	$YFeO_3$	700/900	Yes	[21]
2021	Fortuño	La/Pr/Nd/Sm/Gd	1200	Yes	[22]

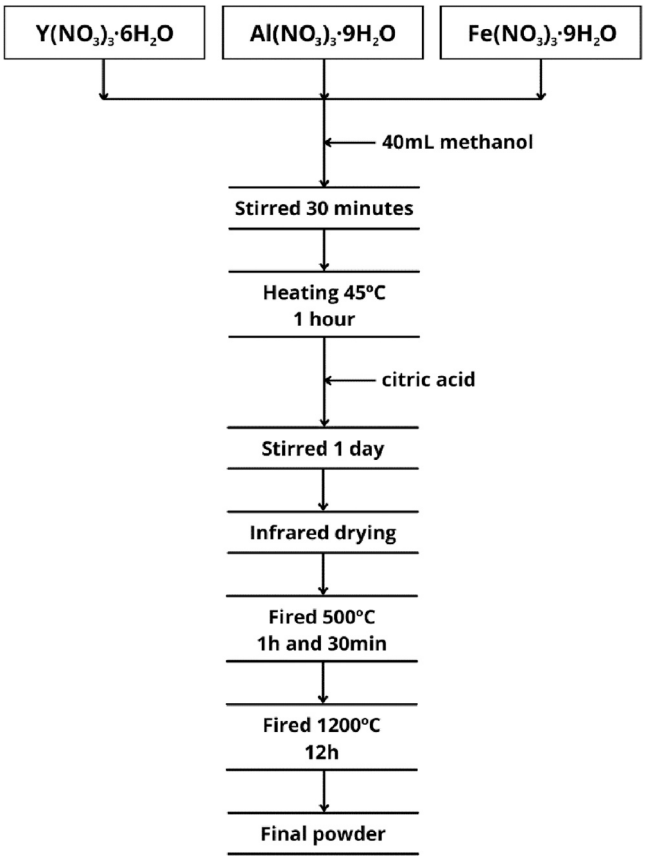

Fig. 1. General scheme of the procedure for the modified Pechini method.

Table 2
Frit composition (wt%).

Composition (wt%)[a]						
SiO_2	Al_2O_3	RO[b]	R_2O[b]	ZnO	PbO	ZrO_2
62.3	10.2	5.9	9.3	3.1	9.1	0.1

[a] The percentages do not represent quantitative analysis
[b] R = alkali or alkaline earth metals

The host network chosen for this work was $YAlO_3$, an orthorhombic perovskite (Pnma space group) with a white colour. The substitution of Al^{3+} by the chromophore ion Fe^{3+} can result in the formation of various solid solutions with intriguing colorations and properties. Additionally, $YAlO_3$ demonstrates excellent thermal stability, with a melting point of approximately 1870 °C and a decomposition temperature exceeding 2000 °C, making it a suitable material for high-temperature applications.

Thus, new environmentally friendly ceramic pigments based on $YAl_{1-x}Fe_xO_3$ were prepared by a modified Pechini method, in an attempt to find interesting colourations for use as multifunctional pigments in different applications, particularly in those that required high temperatures and high NIR-reflectance.

2. Experimental section

2.1. Materials and methods

Different compositions based on $YAl_{1-x}Fe_xO_3$ (x = 0, 0.25, 0.5, 0.6, 0.75, 1) were prepared using a modified Pechini procedure, with Y $(NO_3)_3{\cdot}6\ H_2O$ (99.8%, Sigma-Aldrich), $Al(NO_3)_3{\cdot}9\ H_2O$ (98%, Sigma-

Table 3
Compositions, tolerance factor t and unit cell parameters.

x ($YAl_{1-x}Fe_xO_3$)	t	a (Å)	b (Å)	c (Å)	Volume (Å^3)
0	0.904	14.7310(04)	5.3226(10)	5.1762(10)	405.86(10)
0.25	0.892	14.8450(04)	5.4036(10)	5.2067(15)	417.68(13)
0.5	0.879	14.9670(07)	5.4580(03)	5.2252(20)	426.80(03)
0.6	0.875	15.0260(03)	5.5003(08)	5.2433(09)	433.34(09)
0.75	0.867	11.0700(03)	7.5444(23)	5.2562(16)	438.98(16)
1	0.856	11.1808(18)	7.6013(14)	5.2758(14)	448.39(12)

Aldrich) and $Fe(NO_3)_3{\cdot}9\ H_2O$ (98%, Sigma-Aldrich) as starting reagents. In addition, methanol (99.8%, Scharlab) was used as the solvent, and citric acid (99.5%, Sigma-Aldrich) as the agent to form the polyester.

The corresponding stoichiometric amounts of each reagent were dissolved in 40 ml of methanol, the mixture being stirred for 30 min. The mixture was then transferred into a balloon flask and heated at 45ºC (reflux) for 1 h. The resulting solution was cooled to room temperature and the corresponding amount of citric acid (metal:citric acid, 0.5:1 molar ratio) was added and the mixture was stirred for 1 day. A gel was formed and was subsequently dried under an infra-red lamp. The gel was then fired at 500ºC for 1.5 h to first remove most of the organic matter. Finally, the product was removed from the furnace, ground, placed in a crucible and fired at 1200ºC for 12 h. A general scheme of the method used is shown in Fig. 1.

2.2. Characterization techniques and instrumentation

Phase analysis of the fired samples was performed by powder X-ray diffraction (XRD) with a Bruker-AXS D8 X-ray diffractometer using CuK_α radiation. All data were collected by step-scanning from º2θ = 20–70º at room temperature with a step size of 0.04º and a counting time of 3 s at each step.

Microstructure characterization and semi-quantitative chemical analysis of final powders were performed using a JEOL 7001 F field emission scanning electron microscope (FE-SEM) equipped with an energy dispersive X-ray spectrometer (EDX), and an acceleration voltage of 15 kV. A semi-quantitative analysis was performed based on the EDX results, taking an average of ten measurements in different particles. Samples for microstructure and microanalysis determinations were deposited on a carbon support and sputtered with platinum.

The optical properties of the powder pigments and glazes were measured using a UV-Vis-NIR Jasco V670 spectrophotometer in the 300–2500 nm range with a 1 nm interval, obtaining absorbance and reflectance spectra, as well as the NIR solar reflectance (R_{solar}NIR). This latter value was obtained for each compound by means of Eq. (1), where r(λ) is the spectral reflectance ($W{\cdot}m^{-2}$) measured from UV-Vis-NIR spectroscopy and i(λ) is the standard solar irradiation ($W{\cdot}m^{-2}{\cdot}nm^{-1}$) obtained from ASTM standard G173–03 [23].

$$R_{solarNIR} = \frac{\int_{750}^{2500} r(\lambda){\cdot}i(\lambda)d\lambda}{\int_{750}^{2500} i(\lambda)d\lambda} \quad (1)$$

Reflectance (R_∞) was converted to absorbance (K/S) by the Kubelka-Munk equation: $K/S = 2(1-R_\infty) \times 2\ R_\infty^{-1}$ [24]. The positions of the main absorbed peaks in the optical spectra were determined by a deconvolution procedure (Peak Fitting Module, OringinLab). From the positions of the peaks, the average values of crystal field splitting, Δ_0, by the Tanabe-Sugano diagrams and fitting spin-allowed transitions, and the interelectronic repulsion Racah *B'* parameters were obtained.

CIEL*a*b* and CIEL*C*Hº colour parameters of both the pigments powders and glazes were obtained with a Konica Minolta CM-2300d Portable Spectrophotometer with a beam diameter of 8 mm and using a standard illuminant D65. The chromatic coordinates allowed the pigment to be differentiated in terms of colour based on the following: L* is a measure of lightness and takes values from 0 = black to 100 = white, a* is the green (< 0) to red (> 0) axis, and b* is the blue (< 0) to yellow (> 0) axis. The hue angle (Hº) describes the relative amounts of redness and yellowness and can take values between 0º to 360º: the angle starts from magenta at 0º and shifts towards yellow at 90º, while green and blue are positioned at 180º and 270º, respectively. Chroma (C*) represents the saturation of the colour. Both Hº and C* parameters are related by a* and b* parameters according to Eqs. (2) and (3):

$$H^o = \arctan\left(\frac{b^*}{a^*}\right) \quad (2)$$

$$C^* = \sqrt{a^{*2} + b^{*2}} \quad (3)$$

The thermal stability of the pigments was evaluated by simultaneous thermogravimetry and differential scanning calorimetry (TG-DSC) on a Mettler Toledo analyser (model TGA/DSC3) in the temperature range of 50–1200 ºC, under an air atmosphere, and at a heating rate of 10ºC/min.

The chemical stability of the pigment was studied using acid and alkali solutions and water. 0.25 g of pigment was weighed and dispersed with 5% acid HNO_3, 5% alkali NaOH, and H_2O for 24 h with continuous stirring. The pigment powder was dried, and the CIE colour coordinates were evaluated. The pigment powder was then filtered, washed with deionized water and dried again, and the weight was estimated. The CIE colour coordinates were evaluated and the colour difference (ΔE*) was determined using Eq. (4):

$$\Delta E^* = \sqrt{(\Delta L^*)^2 + (\Delta a^*)^2 + (\Delta b^*)^2} \quad (4)$$

where ΔL*, Δa* and Δb* are the changes in L*, a* and b*, respectively.

2.3. Incorporation of the pigment into a ceramic glaze

The pigment powders at 1200ºC were mixed with a commercial transparent frit (4 wt% of the pigment) using water as a dispersing medium. The frit composition used is given in Table 2. In this way, the interaction of the pigment-frit mixture was studied to find out whether the pigment could be used for colouring ceramic glazes. These mixtures were pressed into pellets with a diameter of 4 cm, placed on a double-fired white body ceramic tile and fired in an electric kiln. The heat treatment applied is equivalent to a standard firing cycle used in the ceramic tile industry where the highest temperature of the cycle was 1080 ºC for 5 min. This cycle involves five steps: ramping to 300ºC in 10 min, heating from 800ºC to the glaze firing temperature in 17 min, holding at 1080 ºC for 5 min, cooling to 600ºC in 20 min, and finally cooling to room temperature in 15 min

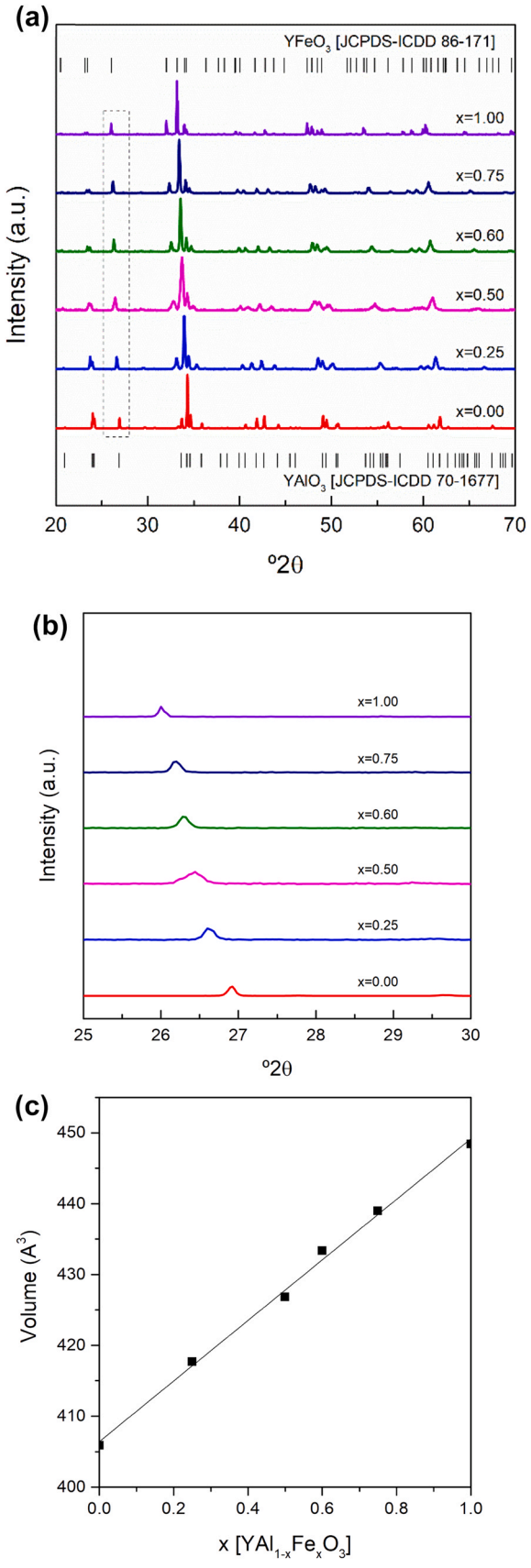

Fig. 2. a) XRD of $YAl_{1-x}Fe_xO_3$ (x = 0, 0.25, 0.5, 0.6, 0.75 and 1); b) Enlargement of the dotted area; (c) Evolution of cell volume with an increasing amount of Fe in the structure.

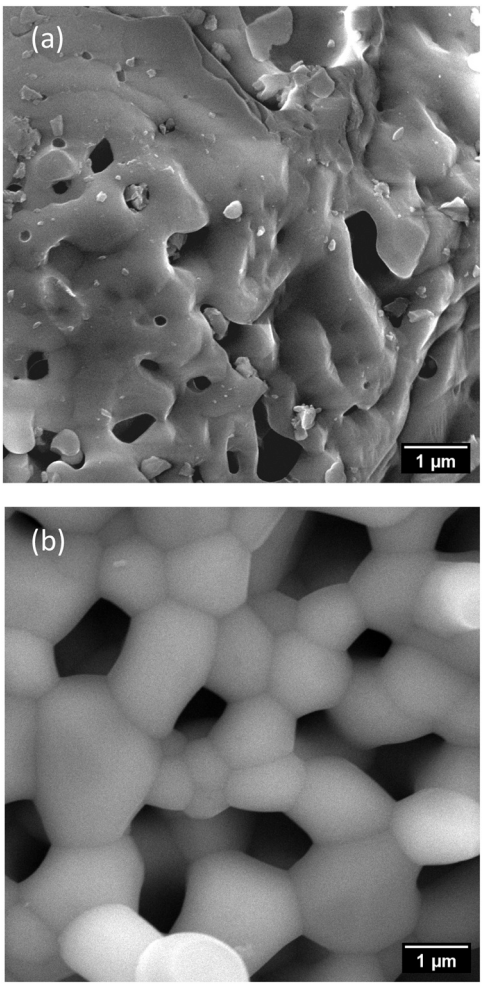

Fig. 3. Images acquired with SEM of the synthesized powder pigments: (a) $YAl_{0.75}Fe_{0.25}O_3$ and (b) $YFeO_3$.

2.4. Evaluation of the compositions as cool pigments

After analysing the reflectance of the different compositions that were prepared, the possibility of using them as cool pigments was studied. To this end, an experiment was carried out in which the variation of the temperature inside a foam structure (5.5 cm × 5.5 cm×7.5 cm; thickness of 0.7 cm) was measured over the passage of time. Specifically, measurements were taken every 5 min for 1 h.

For this purpose, similar previously prepared pigment-frit mixtures were applied to double-fire white bodies, and the pieces were fired at the maximum temperature of 1080ºC with the same standard firing cycle as the one used before (Section 2.3). The pieces were placed on the upper part of the structure and light from an infra-red lamp (Philips, 250 W) was shone on it. A T-type thermocouple was used to measure the temperatures.

3. Results and discussion

Before performing the structural characterization, the Goldschmidt tolerance factor t can also shed some light on the stability and the distortion of the crystal structure. For the compositions that were prepared in which the $YAlO_3$ perovskite was doped at the B site with iron based on the general formula $Y(Al_{1-x}Fe_x)O_{3-\delta}$, the tolerance factor was calculated using Eq. 5:

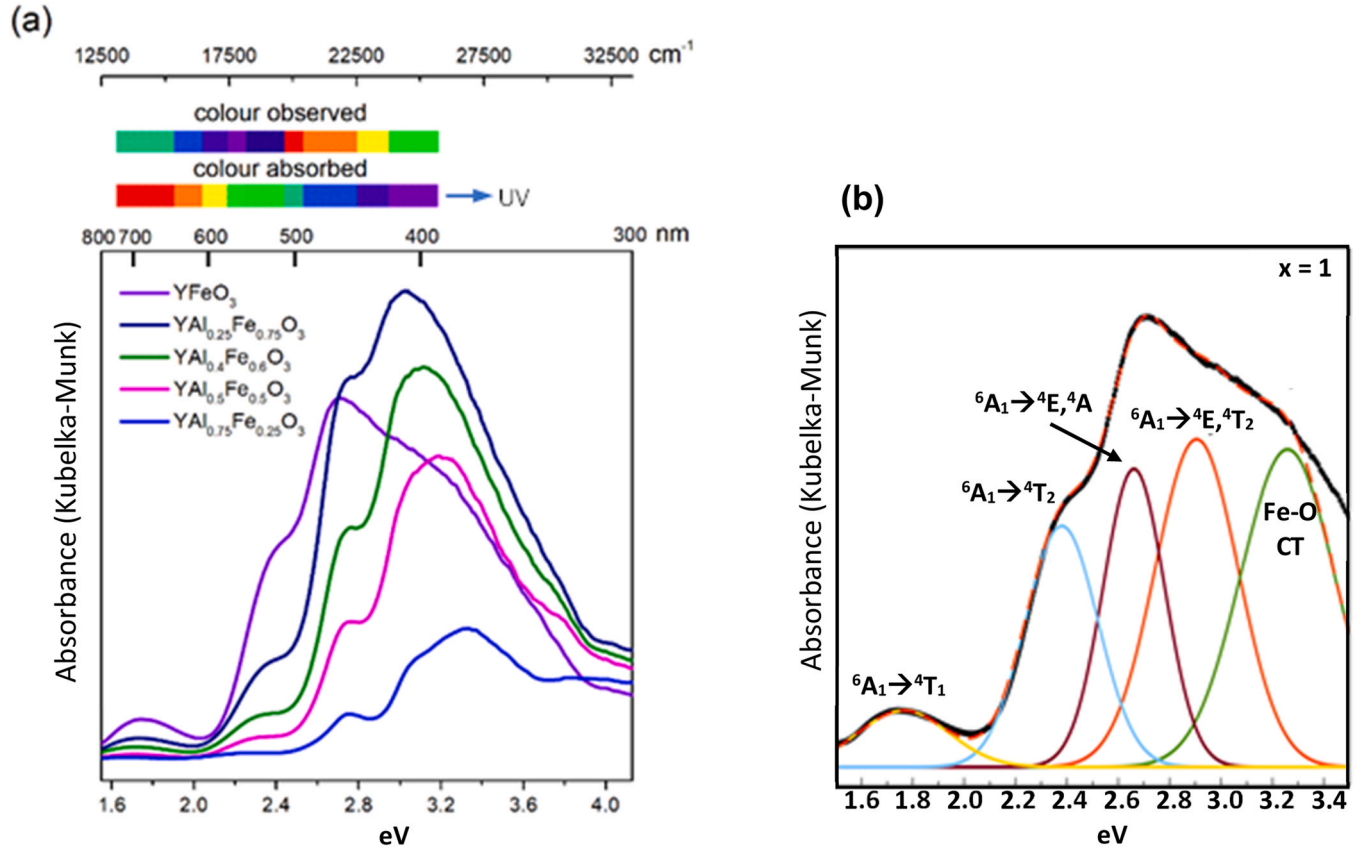

Fig. 4. a) UV-Vis absorption spectra of $YAl_{1-x}Fe_xO_3$ powders; b) UV-Vis absorbance spectrum deconvolution of $YFeO_3$ powder.

Table 4
Wavenumber (cm^{-1}) for the different transitions, Racah parameter (B') and crystal field splitting (Δ_0) values of the $YAl_{1-x}Fe_xO_3$ compounds.

	x = 0.25	x = 0.5	x = 0.6	x = 0.75	x = 1
$^6A_1 \rightarrow {}^4E,{}^4T_2(^4D)$	24570	24331	24213	23980	23364
$^6A_1 \rightarrow {}^4E,{}^4A(^4G)$	22026	22026	21930	21978	21459
$^6A_1 \rightarrow {}^4T_2(^4G)$	18058	18622	18726	19047	19194
$^6A_1 \rightarrow {}^4T_1(^4G)$	13467	13869	13947	14025	2914204
B'	746.14	768.40	773.25	809.9	818.22
Δ_0 (cm^{-1})	12983	13375	13455	14902	15051

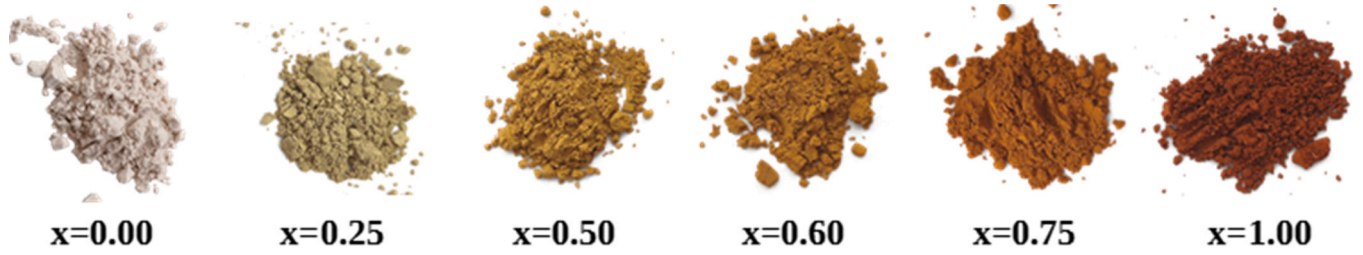

Fig. 5. Photographs of pigment powders.

Table 5
Chromatic coordinates and NIR solar reflectance of the $YAl_{1-x}Fe_xO_3$ powders.

x	L*	a*	b*	C*	Hº	$R_{solarNIR}$ (%)
0.25	78.01	-2.46	26.10	25.71	97.38	55.70
0.5	70.63	5.51	36.09	35.59	82.52	55.52
0.6	63.96	9.47	34.45	37.51	77.95	48.47
0.75	63.78	14.96	37.03	38.42	68.75	47.40
1	55.22	20.20	26.79	32.55	54.35	45.21

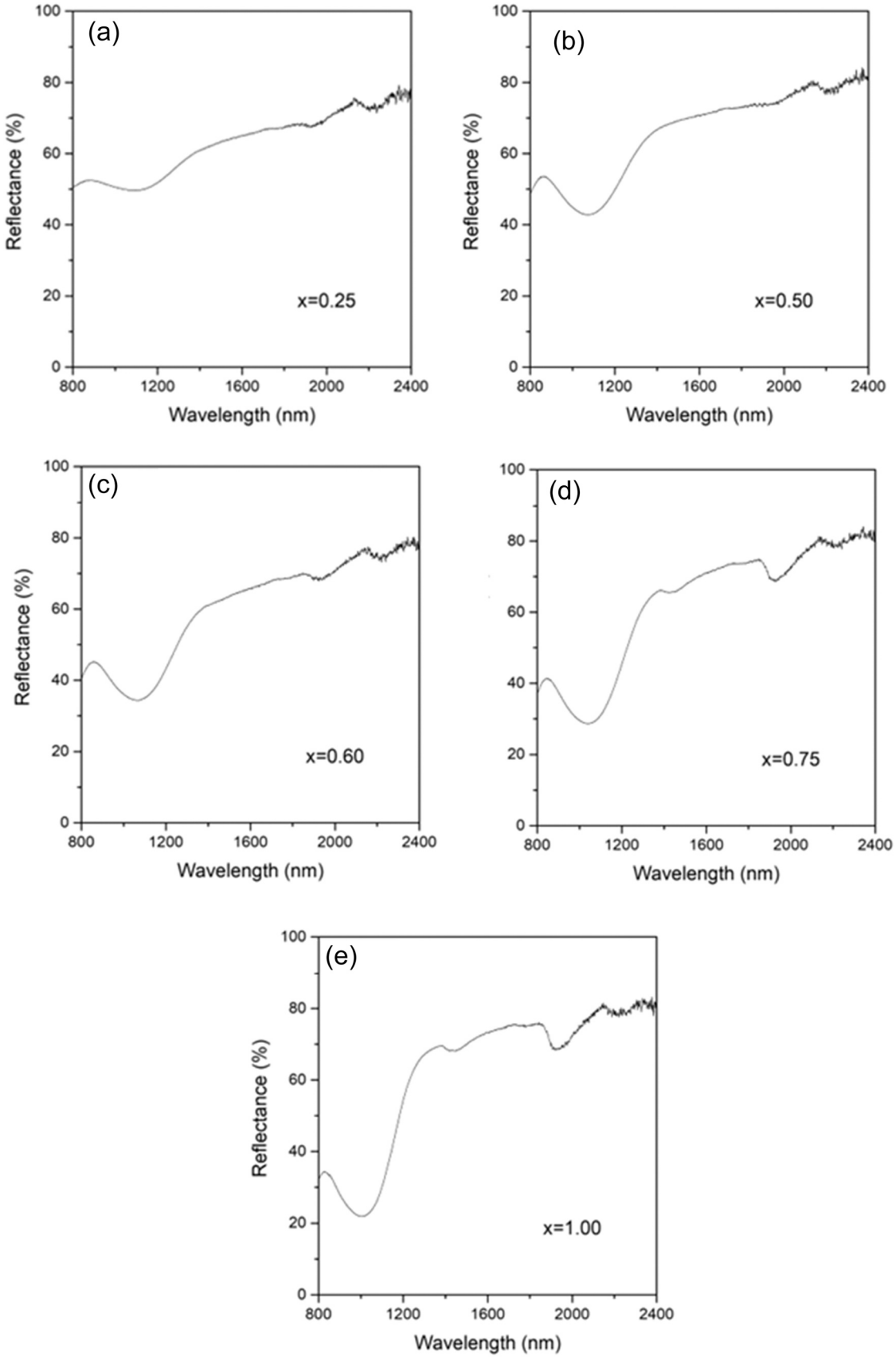

Fig. 6. NIR reflectance spectra of powders.

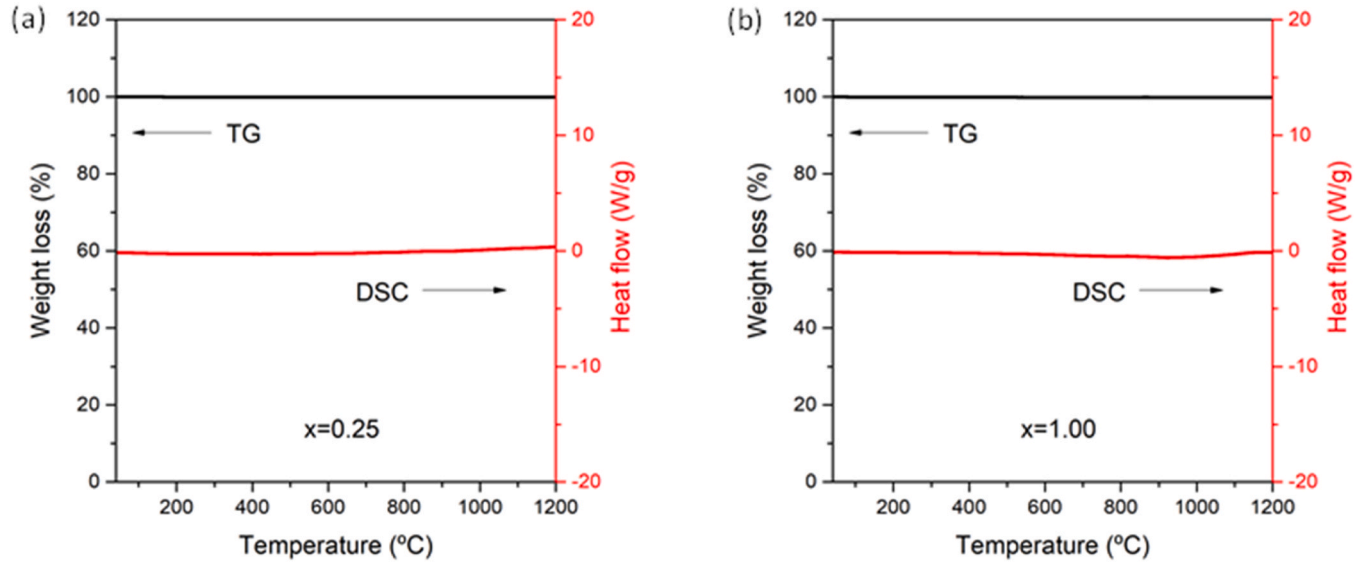

Fig. 7. TG and DSC analysis of pigments: (a) $YAl_{0.75}Fe_{0.25}O_3$ and (b) $YFeO_3$.

$$t = \frac{R_Y + R_O}{\sqrt{2}\left[(1-x)R_{Al} + xR_{Fe} + R_O\right]} \quad (5)$$

where R are the corresponding ionic radii of the different ions involved in this study [25]. For an ideal cubic perovskite, t is close to 1, otherwise it has a distorted structure, such as orthorhombic, rhombohedral or tetragonal [26].

Hence, as can be seen in Table 3, tolerance factors around 0.90 were obtained for all the compositions tested, but this value decreased slightly when iron was incorporated into the structure, thereby suggesting that there was a small distortion of the host lattice in comparison to the undoped compound ($YAlO_3$). In all cases, t was below, but very close to unity. Thus, the AlO_6 and FeO_6 octahedra tilt and rotate leading to closer packing with a Pbnm orthorhombic structure. Notwithstanding, it is important to mention that these results refer to the theoretical nominal formulas proposed in Table 3.

The powders calcined at 1200ºC were characterized by X-ray diffraction (XRD). The XRD patterns for all the compositions that were prepared are shown in Fig. 2(a). The characteristic peaks of the orthorhombic $YAlO_3$ perovskite with the Pnma space group [JCPDS-ICDD 70–1677] were identified in all the compositions synthesized. Therefore, a complete solid solution was obtained. In the case of the last pigment ($YFeO_3$), the theoretical pattern number used was JCPDS-ICDD [86–171]. This code refers to the same phase (orthorhombic perovskite) but with Fe content instead of Al. The positions of the main reflections of each orthorhombic crystalline phase are indicated in Fig. 2(a).

Table 6
Chromatic coordinates and the total colour differences of powder pigments after treatment in the different media.

$YAl_{0.75}Fe_{0.25}O_3$	pH	L*	a*	b*	ΔE*
Air	-	78.01	-2.46	26.10	-
Acid	0.53	77.43	-2.11	25.68	0.79
Alkali	13.69	77.53	-2.29	25.99	0.52
Water	6.62	77.80	-2.41	25.24	0.8826
$YFeO_3$	**pH**	***L****	**a***	**b***	**Δ*E****
Air	-	55.22	20.20	26.79	-
Acid	0.68	54.96	19.79	26.31	0.68
Alkali	13.46	55.04	19.76	26.54	0.53
Water	6.84	54.61	19.97	26.46	0.73

Furthermore, as a larger amount of Fe is introduced into the structure, a shift of the peaks is observed in the diffractograms (Fig. 2b). This shift of the peaks towards lower º2θ is due to the substitution of Al^{3+} cations by Fe^{3+} cations. The Al^{3+} cation has an atomic radius of 53.5 pm (CN = 6), while the Fe^{3+} cation has an atomic radius of 64.5 pm (CN = 6) [19]. If we introduce larger cations into the structure, the distance between the planes of the crystal lattice increases and therefore, according to Bragg's Law, the larger the interplanar distances (d) are, the smaller the diffraction angles (º2θ) will be. This fact can be verified by calculating the cell volume. Table 3 and Fig. 2(c) show a linear increase in cell volume with increasing Fe concentration in $YAlO_3$, thus indicating that as Fe cations larger than those of Al are introduced into the structure, the cell volume increases.

SEM of the different compositions prepared was performed to analyse the microstructure and to determine the evolution of the particle sizes. The microstructures obtained by SEM for compositions x = 0.75 and x = 0 fired at 1200 ºC for 12 h are shown in Fig. 3. The micrographs of the other compositions are shown in Fig S1 of the Supplementary Information (SI). The morphology of the particles of the ceramic powders was similar, showing that in all cases, sintering of the samples had occurred. Furthermore, it is concluded that the greater the amount of aluminium in the composition is, the smaller the grain size is. In addition, on studying different sample regions, EDX revealed that there was no evidence of secondary phases in any of the samples and a homogeneous distribution of the elements in the samples was observed. Each sample presented a similar atomic ratio in the different areas studied.

3.1. Pigment colour evaluation

The optical properties of the compositions prepared were studied using UV-Vis spectroscopy. The absorbance spectra of the fired powders in the 300–800 nm (4.13 – 1.55 eV) range are shown in Fig. 4(a). For these compounds, the $O_{2p} \rightarrow Fe_{3d}$ charge transfer transitions and the 3d-3d transitions of Fe^{3+} are observed in these spectra. All samples presented a similar and typical optical spectrum of Fe(III), dominated by different broad bands that appeared between 2.5 and 3.1 eV (~500–400 nm, in the green-blue region), thus confirming the yellow-reddish colouration. As shown in Fig. 4(b), where the absorbance spectrum deconvolution of $YFeO_3$ is presented as an example, a band was obtained around 3.3 eV (≈375 nm), which corresponds to the $O_{2p} \rightarrow Fe_{3d}$ charge transfer transitions [27].

Fig. 8. Photographs of the pigments with glazes.

Tablee 7
Chromatic coordinates and NIR solar reflectance of the glazes using $YAl_{1-x}Fe_xO_3$ pigments.

x	L*	a*	b*	C*	Hº	$R_{solarNIR}$ (%)
0.25	66.49	-1.02	33.04	32.81	91.80	43.63
0.5	50.84	10.03	29.33	31.07	71.20	39.83
0.6	50.42	12.86	29.31	31.41	66.02	39.29
0.75	41.66	17.73	19.75	27.33	48.81	36.63
1	36.86	22.39	16.66	27.54	36.51	32.86

Moreover, 3d-3d transitions of Fe^{3+} ions generated the other four broad bands found by deconvolution in the range that was studied. The absorption could be attributed to Fe^{3+} d-d intra-atomic transitions which is related to $^6A_1 \rightarrow {}^4E,{}^4T_2(^4D)$ transition (≈2.9 eV, 427 nm), $^6A_1 \rightarrow {}^4E,{}^4A(^4G)$ transition (≈2.66 eV, 466 nm), $^6A_1 \rightarrow {}^4T_2(^4G)$ transition (≈2.38 eV, 520 nm) and $^6A_1 \rightarrow {}^4T_1(^4G)$ transition (≈1.76 eV, 704 nm) in octahedral Fe^{3+} [21,27]. Because the bands were iron-attributed, an increase in band intensity was observed as more Fe was introduced into the compositions reaching a maximum for the sample x = 0.75.

From the absorption bands obtained in the different compositions and the Tanabe-Sugano diagram for d^5, the Racah parameter (B') and crystal field splitting (Δ_0) can be calculated. These values obtained in each composition are included in Table 4. These data are interesting since, from the splitting of the crystalline field, the energy of the different transitions of the compounds can be obtained (Table 4) and the colour variation of the pigments can be explained. The photographs of powders with different compositions are shown in Fig. 5. All these colours arise from electronic transitions between levels whose spacings correspond to the wavelengths available in the visible part of the electromagnetic spectrum. Depending on the different wavelengths absorbed and their intensities, one colour or another is obtained. It is important to remember that it is not the colour associated with these wavelengths that is observed but its complementary one, Fig. 4(a).

To explain the change in pigment coloration, the energy of different transitions has been taken into consideration (Table 4). Based on these transitions, the absorption corresponding to the x = 0.25 sample is weak in the 600–800 nm region (2.06–1.55 eV), which corresponds to the red-orange region. However, more intense absorption bands in the green-blue region (500–400 nm, 2.5–3.1 eV) are observed, resulting in a yellowish coloration perceived by the human eye. As the iron content increases, the intensity of the absorption bands also increases, causing the colour perceived by the human eye to shift towards brown. Finally, for x = 1, the intensity of the bands decreases from 430 nm (2.88 eV) towards the UV region, resulting in a more intense reddish coloration (with reduced absorption in the blue region). In summary, the higher the iron content in the sample, the more reddish the pigment appears.

The decrease in wavelength for the $^6A_1 \rightarrow {}^4T_2$ and $^6A_1 \rightarrow {}^4T_1$ transitions (dependent on the crystal field in d^5 ions) indicates a strengthening or increase in the crystalline field (Δ_0) due to the introduction of the larger Fe(III) ion into the $YAlO_3$ lattice (Table 4). This suggests a change in the coordination environment of Fe(III) and consequently, a distortion of the crystal lattice. As a result, a shift in the energy of the absorption bands in the spectra is observed.

The chromatic properties of the $YAl_{1-x}Fe_xO_3$ pigments, were evaluated by the CIEL*a*b and CIEL*C*Hº parameters listed in Table 5. The decrease in L* values is due to the fact that the sample takes on a darker colour, as it contains more Fe. As regards the other colour coordinates, positive values in b* determine the yellowish hue. Yet, the parameter a* increases as there is a higher amount of iron in the sample. This is reflected visually in a greater perception of the reddish colour in the samples as iron is added (Fig. 5). Similar values of chromatic coordinates (L* and a* around 50 and 20 respectively), were observed for the red-brown Pr-CeO_2 pigments in the literature [11,12]. However, the values of the yellow pigments are slightly lower than those obtained for the Pr-$ZrSiO_4$ yellow pigment (b* around 60) [9,10].

In order to determine the possible application of these pigments as "cool pigments", it is important to determine their NIR reflectance spectra. The NIR reflectance spectra obtained from the glazes coloured with all the pigments that were prepared are shown in Fig. 6. A similar reflectance spectrum is observed in the samples reaching NIR reflectance values of around 70%, the sample of composition x = 0.25 (powder with yellow colouration) being the one with the highest value in the entire NIR interval. These values are similar to those reported in the literature for the previously mentioned pigments with the reflectance in the near-infra-red (R_{NIR}) ranging around 70–75% for both yellow and reddish pigments [9–12]. From these results, the NIR solar reflectance values of the pigment powders were obtained and are presented in Table 5. The NIR solar reflectance values were similar for all compositions, ranging between 55.7% and 45.2%, with the best $R_{solarNIR}$ being the composition with x = 0.25. This fact makes them interesting candidates for use as cool pigments with a significant energy saving performance. Considering all the results, a relationship between the amount of Fe and the NIR solar reflectance is observed. As aluminium is replaced by iron, the NIR solar reflectance values decrease.

3.2. Thermal and chemical stability studies of the pigments

To determine the thermal and chemical stability of the pigments that were developed, a study was carried out on $YAl_{0.75}Fe_{0.25}O_3$ and $YFeO_3$ compounds. These two compositions were chosen because they are at the extremes of the solid solution range studied. In addition, the $YAl_{0.75}Fe_{0.25}O_3$ compound showed the highest NIR solar reflectance and the $YFeO_3$ compound, despite not having such high reflectance, was an interesting candidate to be studied as a cool pigment, and so this type of analysis was also performed.

The thermal stability of two pigments was evaluated by thermogravimetric analysis (TG) and differential scanning calorimetry (DSC) in the temperature range from 50ºC to 1200ºC. Fig. 7 shows the TG and DSC analyses for the two samples studied. As can be seen in this figure, there is no significant change in either curve. This means

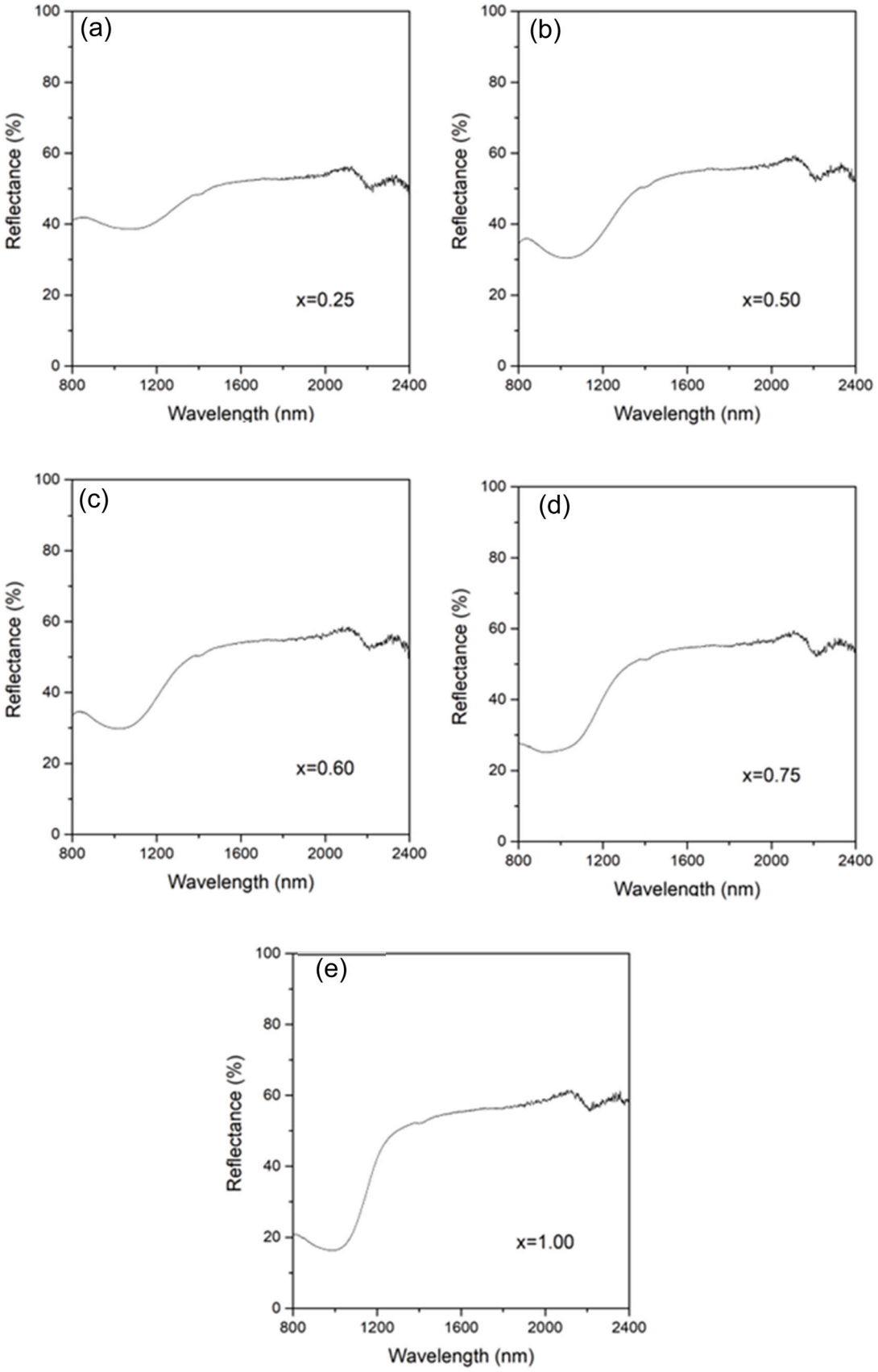

Fig. 9. NIR reflectance spectra of glazes.

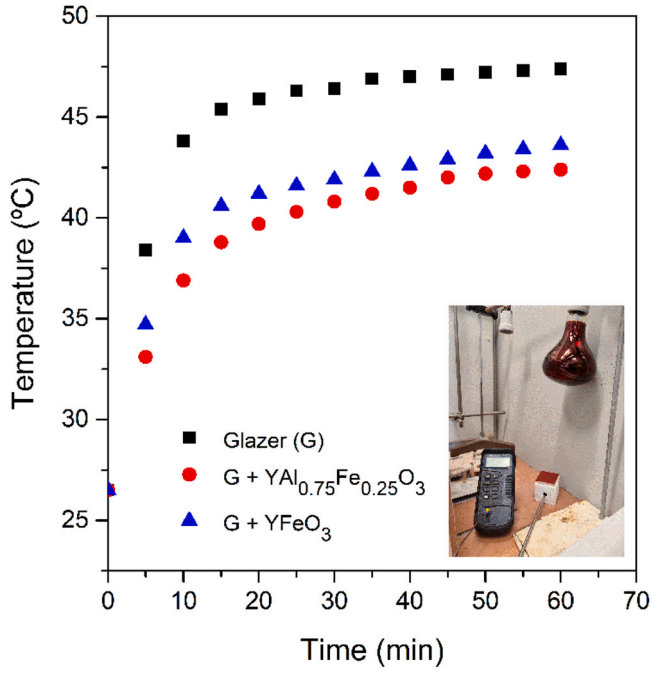

Fig. 10. a) Temperature evolution over time in each glaze; b) Photograph of the assembly used.

that there is no considerable shift in weight or phase transition of the pigment in this temperature range. Thus, it has been demonstrated that the pigments are thermally stable.

To evaluate the chemical stability of these powders, analyses were carried out to determine the resistance to acid, alkali, and water. For both compounds, 0.25 g of pigment was mixed with a 5% HNO_3 solution, 5% NaOH solution and water. It was then left under constant stirring using a magnetic stirrer for 24 h. The chromatic coordinates and the total colour differences (ΔE^*) of the powder pigments after the treatment in the different media are listed in Table 6.

The results obtained show no significant changes in the chromatic coordinates. As a consequence, the ΔE^* parameter takes values lower than the accepted value for the study of the chemical stability of a pigment, which stipulates that a value of ΔE^* greater than 1.2 is indicative of poor chemical stability. Therefore, the $YAl_{0.75}Fe_{0.25}O_3$ and $YFeO_3$ pigments were proven to be chemically stable in acid, alkali, and water media.

Although it is important to know the factors that affect the final colour of the powders, studying their applications in different materials is also fundamental. One of the most common implementations of inorganic pigments is to decorate ceramic tiles by mixing these pigments with a ceramic glaze. If the tiles used to cover the walls or roofs of rooms are decorated with pigments that have high NIR reflectance, that is cool pigments, it can lead to an important reduction in temperature inside the rooms, therefore producing very significant energy savings. It is important to note that the pigments used in ceramic glazes must be stable at high temperatures, since many of the ceramic glaze treatments are carried out at temperatures greater than 1080ºC.

3.3. Evaluation of the colouring performance of the pigments in a ceramic glaze

A pigment should be stable and exhibit an acceptable colorimetric performance when added (and thermally treated when necessary) to different media such as glazes. Therefore, once the powders fired at 1200 ºC had been characterized, their stability and colorimetric performance in a conventional glaze (firing temperature 1080 ºC) was studied. As can be seen in Fig. 8, which shows photographs of the powders after glazing, all the powders presented good stability in the glaze, either maintaining or improving their colour performance. The values of the CIEL*a*b* and CIEL*C*Hº parameters are given in Table 7.

The L* parameter decreases by more than ten units with respect to the powders, which means that the pigments in the glaze give rise to brighter colours. However, parameter a* increases and parameter b* decreases as the amount of iron increases in the composition. This indicates the evolution from yellow for x = 0.25 to red for x = 1.

3.4. Evaluation of the thermal performance of the pigmented glazes

Next, to test the potential application of these pigmented glazes as cooling materials, spectral reflectances in the NIR region were measured. The reflectance spectra for all compositions are shown in Fig. 9. In addition, NIR solar reflectance values, numbered in Table 7, were obtained. A similar reflectance spectrum is observed for all the glazed samples that reach NIR reflectance values of around 55%, a slightly lower value than in the case of powders. On the other hand, all the compositions show high R_{solar}NIR values, but the sample glazed with the $YAl_{0.75}Fe_{0.25}O_3$ pigment (with yellow colouration) is the one showing the highest solar reflectance.

Once it was verified that good reflectance values were obtained, a final study was carried out to test the potential application of these pigments as cool roofing materials. An evaluation of the different indoor air temperature was carried out after a foam building (5.5 cm × 5.5 cm×7.5 cm; thickness of 0.7 cm) was covered with a painted ceramic tile and exposed under an infra-red lamp (Philips, 250 W). The pigments used to colour the glazes for this experiment were the two extremes of the solid solution range ($YAl_{0.75}Fe_{0.25}O_3$ and $YFeO_3$) and a support with the glaze but without pigment was used for comparison. The variation in temperature inside the structures was evaluated over time. A low temperature thermocouple was used to record the temperature at 5 min intervals and the temperatures obtained at the different times for each building are shown in Fig. 10 and Table 8. The inset in Fig. 10 shows the equipment used to test the temperature of the building with the coating of pigmented glazes. At all the times examined, the temperature of the glaze without pigment was higher than the temperature of the pigmented glazes. The unpigmented tile, with only the glaze, reached a temperature of 47.4ºC after one hour. The yellow glaze ($YAl_{0.75}Fe_{0.25}O_3$) maintained a

Table 8
Indoor temperature at variable times for pigmented glazes used as cool roofing material.

Time (min)		10	20	30	40	50	60
Temperature (ºC)*	Glaze (G)_T1	43.8	45.9	46.4	47.0	47.2	47.4
	G + $YAl_{0.75}Fe_{0.25}O_3$ _T2	36.9	39.7	40.8	41.5	42.2	42.4
	ΔT (T1-T2)	6.9	6.2	5.6	5.5	5.0	5.0
	G + $YFeO_3$_T3	39.0	41.2	41.9	42.6	43.2	43.4
	ΔT (T1-T3)	4.8	4.7	4.5	4.4	4.0	4.0

* Initial temperature (0 min) = 26.5 ºC for all measurements.

maximum temperature of 42.4ºC, and the red piece ($YFeO_3$) reached a temperature of 43.6ºC after the same time. This means that by incorporating the pigments in the ceramic glaze, a temperature difference of 5ºC is achieved for the yellow piece and 4ºC for the red glaze. Therefore, given that the interior of a building is lowered by up to 5ºC, the compounds can be referred to as cool pigments.

4. Conclusions

New non-toxic inorganic pigments based on the Fe(III)-doped perovskite $YAlO_3$ structure were synthesized by a modified Pechini method at 1200 °C.

The solubility limit was achieved to reproduce a complete solid solution in the $YAl_{1-x}Fe_xO_3$ system (x = 0, 0.25, 0.5, 0.6, 0.75, 1), a wide range of colourations from yellow to red being obtained, depending on the iron content. Absorption and reflectance measurements in the UV-Vis range confirmed the colouration of these compounds.

Good pigment stability was achieved in a glaze. The pieces coated with the pigmented glazes reached NIR solar reflectance values of 43–32%. The temperature protection studies carried out, with the unpigmented glaze and the pigmented glazes with the compositions $YAl_{0.75}Fe_{0.25}O_3$ and $YFeO_3$, concluded that as a roof coating, the pigmented samples reduced the temperature of a building by 5 °C and 4 °C, respectively, in comparison to the unpigmented glaze.

Thus, the results obtained indicate that these pigments can be excellent candidates for use in high-temperature applications such as colouring ceramic glazes, as well as cool pigments in the walls or roofs of buildings, reducing the energy consumed by air conditioning, improving energy savings and, consequently, contributing to a more sustainable environment.

CRediT authorship contribution statement

All authors contributed equally to perform the required experiments, analyze the data and write the paper. All authors reviewed and edited the manuscript.

Data availability

No data was used for the research described in the article.

Declaration of Competing Interest

The authors declare the following financial interests/personal relationships which may be considered as potential competing interests: Hector Beltran-Mir reports financial support was provided by Spain Ministry of Science and Innovation.

Acknowledgments

H.B-M and E.C. thank the Spanish Ministerio de Ciencia e Innovación [Project PID2020–116149 GB-I00] for the financial support.

Appendix A. Supporting information

Supplementary data associated with this article can be found in the online version at doi:10.1016/j.jallcom.2023.170695.

References

[1] J. Holman, Heat Transfer, McGraw-Hill Publishing Company,, New York, 1990.
[2] H. Akbari, P. Berdahl, R. Levinson, S. Miller, A. Desjarlais, Cool Color Roofing, Materials, University of California,, California, 2006.
[3] The future of cooling, Opportunities for energy-efficient air conditioning. Report of the International Energy Agency (IEA), (2018). www.oecd.org/about/publishing/corrigenda.htm.
[4] T. Thongkanluang, T. Kittiauchawal, P. Limsuwan, Preparation and characterization of Cr_2O_3-TiO_2-Al_2O_3-V_2O_5 green pigment, Ceram. Int. 37 (2011) 543–548, https://doi.org/10.1016/j.ceramint.2010.09.044
[5] R. Levinson, H. Akbari, J.C. Reilly, Cooler tile-roofed buildings with near-infrared-reflective non-white coatings, Build. Environ. 42 (2007) 2591–2605, https://doi.org/10.1016/j.buildenv.2006.06.005
[6] H. Takebayashi, M. Moriyama, Surface heat budget on green roof and high reflection roof for mitigation of urban heat island, Build. Environ. 42 (2007) 2971–2979, https://doi.org/10.1016/j.buildenv.2006.06.017
[7] D.M. Hyde, S.M. Brannon, Investigation of infrared reflective pigmentation technologies for coatings and composite applications, Composites (2006) 1–37.
[8] S. Jose, D. Joshy, S.B. Narendranath, P. Periyat, Recent advances in infrared reflective inorganic pigments, Sol. Energy Mater. Sol. Cells 194 (2019) 7–27, https://doi.org/10.1016/j.solmat.2019.01.037
[9] S. Cerro, M. Llusar, C. Gargori, G. Monrós, Cool and photocatalytic yellow ceramic pigments; from lead-tin to Cr doped scheelite pigments, Ceram. Int. 45 (2019) 4613–4625, https://doi.org/10.1016/j.ceramint.2018.11.150
[10] E. Enríquez, J.J. Reinosa, V. Fuertes, J.F. Fernández, Advances and challenges of ceramic pigments for inkjet printing, Ceram. Int. 48 (2021) 31080–31101, https://doi.org/10.1016/j.ceramint.2022.07.155
[11] N. Masó, H. Beltrán, R. Muñoz, B. Julián, J.B. Carda, P. Escribano, E. Cordoncillo, Optimization of praseodymium-doped cerium pigment synthesis temperature, J. Am. Ceram. Soc. 86 (2003) 425–430, https://doi.org/10.1111/j.1151-2916.2003.tb03316.x
[12] G. Monrós, J.A. Badenes, M. Llusar, Ecofriendly High NIR reflectance ceramic pigments based on rare earths compared with classical chromophores prepared by DPC method, Ceramics 5 (4) (2022) 614–641, https://doi.org/10.3390/ceramics5040046
[13] M. Llusar, J.B. Vicent, J. Badenes, M.A. Tena, G. Monrós, Environmental optimisation of blue vanadium zircon ceramic pigment, J. Eur. Ceram. Soc. 19 (1999) 2647–2657, https://doi.org/10.1016/S0955-2219(99)00041-2
[14] J.D. Cunha, D.M.A. Melo, A.E. Martinelli, M.A.F. Melo, I. Maia, S.D. Cunha, Ceramic pigment obtained by polymeric precursors, Dyes Pigm 65 (2005) 11–14, https://doi.org/10.1016/j.dyepig.2004.06.005
[15] Z. Dohnalová, P. Sulcová, M. Trojan, Synthesis and characterization of LnFeO3 pigments, J. Therm. Anal. Calor. 91 (2008) 559–563, https://doi.org/10.1007/s10973-007-8636-0
[16] P.C. Piña, R. Buentello, H. Arriola, E.N. Nava, Mössbauer spectroscopy of lanthanum and holmium ferrites, Hyperfine Inter. 185 (2008) 173–177, https://doi.org/10.1007/s10751-008-9823-5
[17] C. Piña, H. Arriola, N. Nava, Mössbauer study of iron perovskites of Er, Sm and Nd, J. Phys. Conf. Ser. 217 (2010) 012036. https://doi.org/10.1088/1742–6596/217/1/012036.
[18] O. Opuchovic, G. Kreiza, J. Senvaitiene, K. Kazlauskas, A. Beganskiene, A. Kareiva, Sol-gel synthesis, characterization and application of selected sub-microsized lanthanide (Ce, Pr, Nd, Tb) ferrites, Dyes Pigm 118 (2015) 176–182, https://doi.org/10.1016/j.dyepig.2015.03.017
[19] L. Liu, A. Han, M. Ye, M. Zhao, Synthesis and characterization of Al^{3+} doped $LaFeO_3$ compounds: a novel inorganic pigments with high near-infrared reflectance, Sol. Energy Mater. Sol. Cells 132 (2015) 377–384, https://doi.org/10.1016/j.solmat.2014.08.048
[20] L. Yuan, A. Han, M. Ye, X. Chen, L. Yao, C. Ding, Synthesis and characterization of environmentally benign inorganic pigments with high NIR reflectance: lanthanum-doped $BiFeO_3$, Dyes Pigm 148 (2018) 137–146, https://doi.org/10.1016/j.dyepig.2017.09.008
[21] Y. Li, Y. Ma, W. Liu, Z. Wang, H. Liu, X. Wang, H. Wei, S. Zeng, N. Yi, G.J. Cheng, A promising inorganic $YFeO_3$ pigments with high near-infrared reflectance and infrared emission, Sol. Energy 226 (2021) 180–191, https://doi.org/10.1016/j.solener.2021.08.047
[22] M. Fortuño, P. Serna-Gallén, H. Beltrán-Mir, E. Cordoncillo, A new series of environment-friendly reddish inorganic pigments based on $AFeO_3$ (A=Ln,Y) with high NIR solar reflectance, J. Mater. 7 (2021) 1061–1073, https://doi.org/10.1016/j.jmat.2021.02.002
[23] G. Astm, 173-03: standard tables for reference solar spectral irradiances: direct normal and hemispherical on 37 tilted surfaces. West Conshohocken, PA, ASTM International,, 2003.
[24] S. Marfunin, Physics of Minerals and Inorganic Materials, Springer,, Berlin, Heidelberg, New York, 1979.
[25] R.D. Shannon, Revised Effective Ionic Radii and Systematic Studies of Interatomie Distances in Halides and Chalcogenides. Acta Crystallogr. A32 (1976) 751. http://journals.iucr.org/a/issues/1976/05/00/a12967/a12967.pdf.
[26] J. Saha, Y.M. Jana, G.D. Mukherjee, R. Mondal, S. Kumar, H.C. Gupta, Structure Mössbauer spectroscopy and vibration phonon spectra in valence-bond force-field model approach for distorted perovskites $AFeO_3$ (A = La, Y, Mater. Chem. Phys. 240 (2020) 122286, , https://doi.org/10.1016/j.matchemphys.2019.122286
[27] F. Matteucci, G. Cruciani, M. Dondi, G. Gasparotto, D.M. Tobaldi, Crystal structure optical properties and colouring performance of karrooite $MgTi_2O_5$ ceramic pigments, J. Solid State Chem. 180 (2007) 3196–3210, https://doi.org/10.1016/j.jssc.2007.08.029